Apparent respiratory quotient observed in headspace of static respirometers underestimates cellular respiratory quotient of pear fruit

N. Bessemans[1], P. Verboven[1], B. E. Verlinden[2], M. Janssens[2], M. L. A. T. M. Hertog[1] and B. M. Nicolaï[1,2]

Corresponding author: bart.nicolai@kuleuven.be

[1] *KU Leuven, BIOSYST/MeBioS, Willem de Croylaan 42, 3001 Heverlee, Belgium*

[2] *Flanders Centre of Postharvest Technology, Willem de Croylaan 42, 3001 Heverlee, Belgium*

Abstract

A three-compartment non-equilibrium gas transport model of 'Conference' pear fruit under controlled atmosphere (CA) storage was developed. The model fruit tissue consists of cells, in which the concentrations of respiratory gasses can show gradients, and intercellular space, in which gasses are uniformly distributed. Non-equilibrium of gas concentrations in the cell compartment and intercellular space is assumed. A respiration model based on Michaelis-Menten respiration kinetics without inhibition of respiration by CO_2 and incorporating down-regulation of the maximal O_2 consumption rate in response to O_2 was developed. Conversion of CO_2 dissolved in the cell compartment to hydrogen carbonate at a constant pH of 5.0 was included. The model was validated based on experimental data of 'Conference' pear fruit during a complete depletion experiment starting from 3.58 mol m^{-3} O_2 and 0.00 mol m^{-3} CO_2. Model predictions match experimental observations well. Gas concentrations in the cell compartment were found to be in

equilibrium with the gas concentrations in the intercellular space. The model was used to calculate apparent respiration rates and RQ as if measured in the storage headspace. Apparent values were compared to actual values in the fruit cells and it was found that apparent respiration rates and RQ, calculated based on headspace measurements, underestimated the actual respiration rate and respiratory quotient in the fruit cells. Relative differences of 4 %, 41 % and 41 % were found for the apparent O_2 consumption rate, CO_2 production rate and RQ, respectively. This affects the design of commercial RQ based DCA systems.

Keywords

Dynamic controlled atmosphere, Respiration rate, Mathematical model, non-equilibrium, *Pyrus communis* L.

1 Introduction

After harvest, pear fruit (*Pyrus communis* L.) are often stored at low temperature and under controlled atmosphere (CA) gas conditions to slow down the metabolic and ripening-related processes that lead to quality loss of the fruit (Peppelenbos, 2003; Verboven et al., 2006). Today, pear fruit are almost exclusively stored under static CA conditions in which fruit are stored at a fixed O_2 concentration throughout the whole storage period (Hoehn et al., 2009).

Optimal O_2 concentrations in CA storage for a given cultivar are determined by means of trial and error (Saltveit, 2003). However, the optimal O_2 concentration for a specific batch of fruit depends on the growing conditions and maturity stage of the fruit and may therefore vary for fruit of the same cultivar in a spatially and timely manner (Dilley, 2010; Gasser et al., 2010). As a result, conventional CA storage often leads to more quality loss than expected as the O_2 concentration in storage might be higher or lower than the anaerobic compensation point (ACP) - the O_2 concentration at which the CO_2 production of the fruit is minimal (Boersig et al., 1988).

As a solution, dynamic controlled atmosphere (DCA) storage was developed. With DCA, the O_2 concentration in-storage is dynamically adapted towards the lower O_2 limit of the fruit, based on measurements of a biological response of the stored fruit to low O_2 stress (Wolfe et al., 1993). In this way, fruit respiration and ethylene production is minimized, leading to maximal quality retention while avoiding off-flavors and storage disorders associated with fermentation. One type of DCA developed is the dynamic control system (DCS) which uses ethanol measurements of the headspace in a small box of sample fruit that is positioned inside the storage environment as a response to low O_2 stress (Prange et al., 2002; Schouten et al., 1997; Veltman et al., 2003). However, due its high solubility in water, ethanol accumulates in the fruit and the majority of ethanol formed remains in the fruit (Gupta et al., 2000; Knee and Hatfield, 1976), making detection difficult. Furthermore, ethanol produced can be re-metabolized to acetaldehyde and ethyl esters by other fruit, leading to an underestimation of the low O_2 stress experienced by the fruit (Pesis et al., 2002). Another DCA system, based on chlorophyll fluorescence has been developed (DCA-CF) (DeLong et al., 2004). With DCA-CF, the chlorophyll fluorescence of the fruit skin of a sample of 6 fruit placed in a small container is used to detect low O_2. This implies the need of placing many sample containers in a storage room to have enough samples to represent the O_2 stress level of the entire room. Additionally, peaks in chlorophyll fluorescence can be caused by other types of stress than low O_2 stress, such as chilling stress and CO_2 stress (Ogren, 1990; Wright et al., 2010).

RQ-DCA uses measurements of the RQ of the stored fruit as bio response to detect low O_2 stress. RQ is defined as the ratio of the CO_2 production rate to the O_2 consumption rate of the fruit (Fonseca et al., 2002). Under aerobic conditions, RQ has a value close to 1.0, but increases exponentially at low O_2 concentrations when the fruit metabolism shift from aerobic respiration to fermentation (Ho et al., 2013; Yearsley et al., 1996). The principle of using RQ as a biological

response to detect low O_2 stress has been known for many years (Wollin et al., 1985; Wolfe et al., 1993), but had not been used commercially as gas leakage of the storage environment corrupts the measurements. This problem was solved by the development of a model-based leak correction measurement, allowing real-time correction of measured RQ-values for leakage of the storage environment (Bessemans et al., 2018) and, alternatively, by the enclosure of fruit in RQ measurement chambers within or connected to the CA room (Schaefer and Bishop, 2014; Brackmann, 2015) .

Today, an increasing amount of publications report on the performance of RQ-DCA storage on maintaining fruit quality and aroma biosynthesis (Bessemans et al., 2016; Both et al., 2017; Oliveira et al., 2018). In all work reported, it is assumed that the fruit-environment system is in steady-state and that respiration rates of O_2 and CO_2 measured in the headspace of the storage facility represent the respiration rates inside the fruit cells (Burg and Burg, 1965; Gran and Beaudry, 1993; Yearsley et al., 1996). Hereby, it is assumed that all CO_2 produced by the cells immediately diffuses out of the fruit and that O_2 consumed by respiration in the cells diffuses instantaneously from the storage headspace through the fruit cortex tissue and into the cells. In practice, respiration rates are calculated from measured changes in gas concentrations over time, implying that steady-state conditions can never be met. Previous modelling efforts by Ho et al. (2010) have shown that the fruit skin is the main resistance to gas exchange between fruit and storage environment, creating a large concentration difference between the gas concentrations in- and outside the fruit. Inside the fruit, the cortical parenchyma tissue consists of a matrix of two phases, namely the fruit cells and intercellular space, which facilitate gas exchange between fruit cells and environment (Herremans et al., 2015a, 2015b). Until recently, it was thought that due to the bulkiness of the fruit and, thus, the resistance of the fruit cortex tissue to transport of O_2 and

CO_2 gas, internal gradients in the concentrations of these gasses were present in the fruit (Ho et al., 2013, 2010). Recently, Ho et al. (2018) demonstrated that in 'Conference' pear fruit, internal gradients in gas concentrations became more shallow, when respiration decreased due to low temperature or decreasing O_2 concentrations. However, they assumed the gas concentrations in the intercellular space and in the cell compartment phase inside the fruit tissue was in equilibrium, which mathematically forces the gas in or out the fruit cells depending on Henry's law (Rosenberg and Peticolas, 2004).

Under aerobic conditions cellular RQ is equal to 1.0 when hexoses are used as substrates in the respiration process. Deviations varying from 0.7 to 1.3; when lipids are used as a substrate, RQ values will be lower than 1.0, and when organic acids are used as substrate, they will be greater than 1.0 (Kader, 1997; Cameron et al., 1994; Renault et al., 1994; Saltveit 2019). In RQ-DCA storage, RQ measurements were observed that deviate more from 1.0 than could biochemically explained. An explanation for observed RQ-values greater than 1.3 was found in the leak of O_2 gas into the storage room during RQ-measurement (Bessemans et al., 2018). However, in RQ-DCA storage, RQ values lower than 0.7 were observed, which remain inexplicable until now.

The hypothesis of this work is that the apparent respiration rates and RQ, determined based on measured changes in gas concentrations in the headspace of the storage environment, underestimate the actual respiration rates and RQ in the fruit cells in static storage environments due to the difference in solubility and transport properties of O_2 and CO_2 in the fruit tissue. The following objectives were targeted to evaluate the hypothesis:

1. Development of a lumped three-compartment non-equilibrium gas transport model describing the O_2 and CO_2 gas exchange between pear fruit and their storage environment.

By lumped it is meant that no internal gas gradients occur inside the fruit, so that at every point inside the fruit volume the local concentration equals the average concentration inside the fruit;

2. Estimate necessary model parameters and validate the developed model based on experimental data;
3. Use the validated model to evaluate the assumption of equilibrium between the gas and cell compartment phase in the fruit;
4. Use the validated model to compare actual O_2 consumption, CO_2 production rates and RQ in the fruit cells to the apparent estimated respiration rates and RQ observed in the storage headspace.

2 Materials and methods

2.1 Three-compartment gas exchange model

We developed a gas exchange model of fruit that can simulate the gas exchange dynamics of fruit with a confined environment. The model incorporates three compartments: the confined environment headspace (e.g. storage room or respiration jar), the intercellular space and the cellular compartment.

Consider a stack of fruit in a confined environment. The headspace compartment is defined as the free space between the fruit in the confined storage space and contains the storage atmosphere. The intercellular pores compartment is defined as the space inside the fruit in between the fruit cells. Finally, the cellular compartment is defined as the space occupied by the cells inside the fruit. When completely airtight, the rate of change of respiratory gasses in the storage atmosphere depends on the resistance of the fruit skin to gas transport as this is the rate limiting factor of gas

exchange between fruit and environment. Assuming that the atmosphere in the storage volume is perfectly mixed and gas exchange between fruit and environment occurs via the intercellular space of the fruit, the mass rate of change of respiratory gasses in the storage headspace is given by:

$$\begin{cases} V_a \dfrac{dc_{O_2,a}}{dt} = -h_{O_2,s} A_s \left(c_{O_2,a} - c_{O_2,g} \right) \\ V_a \dfrac{dc_{CO_2,a}}{dt} = -h_{CO_{2,s}} A_s \left(c_{CO_2,a} - c_{CO_2,g} \right) \end{cases} \quad (1)$$

where V_a represents the volume of the storage atmosphere [m^3], $c_{i,a}$ the concentration of component *i* (O_2 or CO_2) in the storage atmosphere [mol m^{-3}], $h_{i,s}$ the permeability of the fruit skin for component *i* [m s^{-1}], A_s the total surface area of skin of the fruit [m^2] and $c_{i,g}$ the concentration of gas component *i* in the intercellular space of the fruit [mol m^{-3}]. The skin permeability can be calculated as:

$$h_{i,s} = \frac{1}{\frac{\delta_s}{D_{i,s}}} \quad (2)$$

with δ_s the average thickness of the fruit skin [m] and $D_{i,s}$ the diffusivity of gas component *i* in the fruit skin [m^2 s^{-1}].

Due to the extensive network of intercellular space, the gas inside the fruit cortex may be assumed to be uniformly distributed around the fruit cells, without occurrence of gradients in the gas concentrations in the intercellular spaces (Herremans et al., 2015b; Ho et al, 2018). The volume integrated rate of concentration change of respiratory gases in the intercellular space, is, therefore, equal to the sum of the gas exchange between the intercellular space and the storage environment and the gas exchange between the intercellular space and the fruit cells:

155
$$\begin{cases} \varepsilon V_f \dfrac{dc_{O_2,g}}{dt} = -h_{O_2,s} A_s \left(c_{O_2,g} - c_{O_2,a} \right) - h_{O_2,cell} A_{cortex} V_f \left(c_{O_2,g} RTH_{O_2} - c_{O_2,cell} \right) \\ \varepsilon V_f \dfrac{dc_{CO_2,g}}{dt} = -h_{CO_2,s} A_s \left(c_{CO_2,g} - c_{CO_2,a} \right) - h_{CO_2,cell} A_{cortex} V_f \left(c_{CO_2,g} RTH_{CO_2} - c_{CO_2,cell} \right) \end{cases} \quad (3)$$

156 with ε the porosity of the fruit cortex tissue [-], $h_{i,cell}$ the permeability of the cells for component
157 i [m s^{-1}], A_{cortex} the specific area of the fruit cortex tissue [m^2 m^{-3}], V_f the fruit volume [m^3], R the
158 universal gas constant [J mol^{-1} K^{-1}], T the temperature [K], H_i the Henry constant of component
159 i in the cell compartment at 0 °C [mol m^{-3} Pa^{-1}] and $c_{i,cell}$ the concentration of component i in the
160 fruit cells [mol m^{-3}]. Note that although no equilibrium is assumed between the gas concentrations
161 in the cells and the intercellular space, local equilibrium is assumed at their interface using Henry's
162 law.

163 During transition of gas molecules from the intercellular space to the fruit cells and vice versa, the
164 cell wall, cell membrane and cell compartment provide the main resistances to gas transport.
165 Assuming spherical cells, the permeability of the cells for component i can be calculated from
166 these resistances in series and is given by:

167
$$h_{i,c} = \frac{1}{\frac{\delta_{cw}}{D_{i,cw}} + \frac{\delta_{cm}}{D_{i,cm}} + \frac{0.75 R_{cell}}{D_{i,cell}}} \quad (4)$$

168 with δ_{cw} the thickness of the cell wall [m], $D_{i,cw}$, the diffusivity of gas component i in the cell wall
169 [m^2 s^{-1}], δ_{cm} thickness of the cell membrane [m], $D_{i,cm}$, the diffusivity of gas component i in the
170 cell membrane [m^2 s^{-1}], R_{cell} the average spherical equivalent radius of the pear cells [m], $D_{i,cell}$,
171 the diffusivity of gas component i in the cell compartment [m^2 s^{-1}]. As the cells are assumed to be
172 spherical, if internal gas concentration gradients occur, at the radial position from the cell centre

equal to 0.25 times the cell radius, the gas concentrations is equal to the average concentration in the fruit cell (Smith and Bennet, 1965). Therefore 0.75 of the cell radius was used to calculate the resistance of the cell compartment to gas transport. An schematic representation of the fruit skin- and cell resistance to gas transport is depicted in Figure 1.

Gasses in the cell compartment are associated with fruit respiration. In the respiration process, O_2 is consumed while CO_2 is produced. Furthermore, CO_2 dissolved in the cell compartment may be converted into H_2CO_3 and further to HCO_3^-, depending on the pH of the cell compartment. Therefore, the volume integrated rates of change of the concentrations of the respiratory gasses in the cell compartment are given by:

$$\begin{cases} (1-\varepsilon)V_f \dfrac{dc_{O_2,cell}}{dt} = h_{O_{2,cell}} A_{cortex} V_f \left(c_{O_{2,g}} RTH_{O_2} - c_{O_2,cell} \right) + r_{O_2} (1-\varepsilon) V_f \\ (1-\varepsilon)V_f \dfrac{dc_{CO_2,cell}}{dt} = h_{CO_{2,cell}} A_{cortex} V_f \left(c_{CO_{2,g}} RTH_{CO_2} - c_{CO_2,cell} \right) + r_{CO_2} (1-\varepsilon) V_f + S_{CO_2} (1-\varepsilon) V_f \end{cases} \quad (5)$$

where r_{O_2} represents the rate of O_2 consumption by respiration [mol m^{-3} s^{-1}], r_{CO_2} the rate of CO_2 production by respiration [mol m^{-3} s^{-1}] and S_{CO_2} a volumetric source term accounting for the (re)conversion of dissolved CO_2 to HCO_3^- [mol m^{-3} s^{-1}]. This volumetric source term links the CO_2 equation of the cell compartment to the equation describing the mass rate of change of the concentration of HCO_3^-, given by:

$$(1-\varepsilon)V_f \frac{\partial c_{HCO_3^-}}{\partial t} = -S_{CO_2} (1-\varepsilon) V_f \quad (6)$$

with $c_{HCO_3^-}$ the concentration of HCO_3^- in the cell compartment [mol m^{-3}].

2.2 Respiration model

In previous work (Ho et al. 2018, Lammertyn et al., 2001 and Lammertyn et al., 2003), Michaelis-Menten respiration models of intact fruit or fruit tissue disks were developed to simulate fruit respiration behavior. The model parameters estimated in these modeling approaches are not suitable to model respiration, as the Michaelis-Menten constants also contain information about the macroscopic diffusion of gas through the fruit tissue (Lammertyn et al., 2001). Therefore, in this work a cellular respiration model was used A Michaelis-Menten model with non-competitive inhibition of respiration by CO_2 (Hertog et al., 1998; Ho et al., 2010; Lammertyn, 2001) was used to describe the consumption of O_2 by respiration as given by:

$$r_{O_2} = \frac{V_{m,O_2} c_{O_2,cell}}{\left(K_{m,O_2} + c_{O_2,cell}\right)} \tag{7}$$

with V_{m,O_2} the maximal rate of O_2 consumption by respiration [mol m^{-3} s^{-1}], K_{m,O_2} the Michaelis-Menten constant of respiration [mol m^{-3}].

The equation for CO_2 production by respiration consists of an oxidative and a fermentative part (Peppelenbos, 1996):

$$r_{CO_2} = RQ_{ox} r_{O_2} + \frac{V_{m,f,CO_2}}{\left(1 + \frac{c_{O_2,cell}}{K_{m,f,O_2}}\right)} \tag{8}$$

with RQ_{ox} the respiratory quotient of fruit cells under aerobic conditions [-], V_{m,f,CO_2} the maximal fermentative rate of CO_2 production [mol m^{-3} s^{-1}], and K_{m,f,O_2} the Michaelis-Menten constant of fermentation [mol m^{-3} s^{-1}].

A value for K_{m,O_2} of pear protoplasts was obtained from Lammertyn et al. (2001). Our model, assumed a RQ_{ox} value of 1.0, representing fully oxidative respiration of hexoses (Andrich, 2006). Other model parameters for respiration were not found in literature and were estimated by fitting the model to experimental data obtained from experiments described in Section 2.4.

The response of fruit respiration to external O_2 concentrations was taken into account following the approach proposed by Ho et al. (2018) who assumed changing O_2 concentrations to cause a signal transduction cascade, resulting in a change in the enzymes involved in respiration and so in V_{m,O_2}. Under thesis circumstances, the rate of change of V_{m,O_2} is given by:

$$\begin{cases} \dfrac{dV_{m,O_2}}{dt} = k_d \left(V_r - V_{m,O_2} \right) \\ V_r = V_{r,1} + \dfrac{\left(V_{r,2} - V_{r,1} \right) c_{O_2,cell}^2}{K_H + c_{O_2,cell}^2} \end{cases} \quad (9)$$

with k_d the rate of response of V_{m,O_2} to changing O_2 concentrations [s^{-1}], K_H the sensitivity of V_{m,O_2} to the O_2 concentration [$mol^2\ m^{-6}$], $V_{r,2}$ the maximal rate of O_2 consumption under aerobic conditions [mol m^{-3} s^{-1}], $V_{r,1}$ the basal maximal O_2 consumption rate [mol m^{-3} s^{-1}], V_r the maximal O_2 consumption rate at a steady state O_2 concentration [mol m^{-3} s^{-1}] and $\left(V_{r,2} - V_{r,1} \right)$ the amplitude of regulation of V_{m,O_2} by the O_2 concentration [mol m^{-3} s^{-1}].

2.3 CO_2 conversion model

CO_2 dissolved in the cell compartment can react with water, resulting in formation of H_2CO_3, which is a weak acid (pK_a = 6.35) and which, depending on the pH of cell compartment, can dissociate in HCO_3^- and H^+ according to:

226 $$CO_2 + H_2O \underset{k_2}{\overset{k_1}{\rightleftarrows}} H_2CO_3 \overset{K}{\rightleftarrows} HCO_3^- + H^+$$

227 with k_1 the CO_2 hydration constant (s^{-1}), k_2 the dehydration constant of HCO_3^- (s^{-1}) and K the acid
228 dissociation constant of H_2CO_3 (mol m^{-3}). From this equilibrium reaction, a volumetric source term
229 S_{CO_2} can be derived describing the formation/reaction of CO_2 dissolved in the cell compartment:

230 $$S_{CO_2} = k_2 \frac{c_{HCO_3^-} c_{H^+}}{K} - k_1 c_{CO_2} \quad (10)$$

231 where $c_{HCO_3^-}$ represents the concentration of HCO_3^- in the cell compartment (mol m^{-3}), c_{H^+} the
232 concentration of H^+ in the cell compartment (mol m^{-3}). Inside the fruit cortex tissue cells, the pH
233 of the cytosol is buffered at a constant value of 7.0, which is the normal pH of plant cells (Kurkdjian
234 et al., 1978; Roberts et al., 1982). Contrary, in the vacuole, due the high abundance of organic
235 acids, the pH is much lower (Smith and Raven, 1979). The vacuole makes up to 90 % of the cellular
236 volume (Nobel, 1991). The overall pH of the cell compartment of the pear cells in our model was
237 assumed to be equal to 5.0, which is the pH of pear juice (Lide 1999). The solubility of CO_2 in the
238 cellular liquid depends mainly on the pH as dissolved CO_2 may react with water to form H_2CO_3,
239 which can dissociate to form HCO_3^-. Sensitivity analysis on the effect of pH on the ratio of HCO_3^-
240 and CO_2 concentrations in the liquid phase in the cells by Ho et al. (2009) indicated that at pH 7
241 (cytosolic pH) or pH 4.82 (vacuolar pH) almost all CO_2 in the cellular liquid is present in the form
242 of CO_2, the ratio of $c_{HCO_3^-}$ to c_{CO_2} in the vacuole varied from 0.0367 to 0.0544 while in cytoplasm
243 this ratio varied from 0.0516 to 0.163. Therefore changes in pH this region will affect model
244 outcome on CO_2 concentrations very little. Moreover, due to the high diffusivity of H^+ (9.3×10^{-9}
245 $m^2\ s^{-1}$), pH in the vacoule may be assumed to be constant and uniform (Ho et al., 2009). As a

246 concequence, it is very unlikely that the pH and solubility of CO_2 in the cellular liquid changes
247 significantly, especially during the short period of 11 d this experiment.

248 2.4 Determination of respiration model parameters

249 Experiments were conducted to obtain experimental data to fit the model and obtainestimates of
250 the respiration model parameters. 'Conference' pear fruit were placed in 5 glass jars (2 fruit per
251 jar) with a volume of 1.7 L, acting as static respirometers. On average, the fruit-headspace volume
252 ratio of the jars was 0.45 ± 0.036. The fruit volume was determined using Archimedes' principle,
253 while the volume of the jars was determined using their empty weight and their weight when filled
254 with water at known temperature. The intercellular pore spaces are included in the fruit volume as
255 they are part of the fruit. Headspace volume was finally calculated by subtracting the volume of
256 the fruits from the empty jar volume for each individual jar. Jars were closed airtight, placed in a
257 dark cold room at 0 °C and flushed with a gas mixture of 3.58 mol m^{-3} (8.0 kPa) O_2 and 0.0 mol
258 m^{-3} (0.0 kPa) CO_2 for a period of 24 h, using an in-house built gas mixing pannel. Subsequently,
259 gas fractions in the jars were measured once a day for a period of 11 d using a portable gas analyzer
260 (Checkmate II, PBI, Dansensor, Denmark). The gas analyzer had an accuracy of ± 0.1 % and ± 0.5
261 % of the O_2 reading and CO_2 reading, respectively. The analyzer was calibrated against calibrated
262 mixtures (Air Products N.V., Belgium). Along with daily gas fraction measurements, jar pressure
263 was measured using a portable pressure sensor (DPI 142, GE Druck, Germany) with an accuracy
264 of ± 0.01 % of the reading. Measured changes in gas fraction and pressure were used to calculate
265 molar gas concentrations and respiration rates expressed in mol per m^3 fresh volume of sample
266 and per s using the ideal gas law. The obtained gas concentrations over time were used to fit the
267 gas exchange model (equations (1), (3), (5) and (6)) and thus obtain estimates for the respiration
268 model parameters of equations (7), (8) and (9), except K_{m,O_2} and RQ_{ox} that were obtained from

literature. Optimization of the model parameters was conducted in OptiPa (Hertog et al., 2007), a dedicated optimization tool which was developed using Matlab (The MathWorks, Inc., Natick, MA, USA). Differential equations were solved using the Matlab ode15s solver for stiff equations and the model parameters were estimated using non-linear least squares optimization making use of the Levenberg–Marquardt method.

2.5 Evaluation of non-equilibrium assumption

To evaluate the assumption of non-equilibrium between gas concentrations in the cell compartment and those in the intercellular pore space, concentrations of O_2 and CO_2 in the cell compartment, simulated using the non-equilibrium model, were compared to the concentrations of O_2 and CO_2 in the cell compartment calculated under the assumption of equilibrium. At a constant temperature of 0 °C as during the experiment, Henry's law can be used to calculate equilibrium gas concentrations in the cell compartment from the gas concentrations in the gas in the intercellular space. Henry's law states that the amount of a gas dissolved in a liquid with a fixed volume, is directly proportional with the concentration of that gas in equilibrium with the liquid (Rosenberg and Peticolas, 2004). Therefore, concentrations of O_2 and CO_2 in the cell compartment under the equilibrium assumption were carculated as:

$$\begin{cases} c_{\mathrm{O}_2,cell}^{eql} = c_{\mathrm{O}_2,g} RTH_{\mathrm{O}_2} \\ c_{\mathrm{CO}_2,cell}^{eql} = c_{\mathrm{CO}_2,g} RTH_{\mathrm{CO}_2} \end{cases} \quad (11)$$

with $c_{\mathrm{O}_2,cell}^{eql}$ and $c_{\mathrm{CO}_2,cell}^{eql}$ the concentration of O_2 and CO_2, respectively, in the cells under the assumption of equilibrium with the intercellular space [mol m^{-3}].

2.6 Calculation of cellular and headspace respiration rates and RQ

289 To compare simulated actual respiration rates and RQ in the cell compartment to the simulated
290 and measured apparent respiration rates and RQ in the headspace of the jars, the validated model
291 was used to simulate the depletion experiment for a respiration jar with the avarage fruit-to-
292 headspace volume ratio of 0.45 used in the experiments. Values of the actual respiration rates in
293 the cell compartment were calculated using the respiration model given by equations (7-8), while
294 the actual RQ of the pear cells was calculated by taking the ratio of the cellular CO_2 production
295 rate and O_2 consumption rate, *i.e.*:

296 $$RQ_{cell} = \frac{r_{CO_2}}{r_{O_2}} \tag{12}$$

297 where RQ_{cell} represents the cellular respiratory quotient.

298 Apparent simulated O_2 consumption rate and CO_2 production rate in the headspace of the jar were
299 calculated as:

300 $$r_{O_{2,a}} = \left| \frac{V_a}{V_f \left(1-\varepsilon\right)} \frac{d}{dt} c_{O_2,a} \right| \tag{13}$$

301 and

302 $$r_{CO_{2,a}} = \left| \frac{V_a}{V_f \left(1-\varepsilon\right)} \frac{d}{dt} c_{CO_2,a} \right| \tag{14}$$

303 where $r_{O_{2,a}}$ represents the apparent O_2 consumption rate in the headspace of the jar [mol $m^{-3}s^{-1}$] and
304 $r_{CO_{2,a}}$ the apparent CO_2 production rate in the headspace of the jar [mol m^{-3} s^{-1}]. Note that the factor
305 $\left(1-\varepsilon\right)$ corrects for the fact that not the whole fruit volume consists of fruit cells, but also partially
306 of intercellular space.

307 Values of the apparent respiratory quotient in the headspace of the jar were calculated as:

308 $$RQ_a = \frac{r_{CO_2,a}}{r_{O_2,a}} \quad (15)$$

309 where RQ_a represents the apparent respiratory quotient calculated from concentration changes in
310 the headspace of the jar.

311 Experimental respiration rates were calculated based on the measured concentrations profiles of
312 O_2 and CO_2 gas during the depletion experiments described in Section 2.4. Hereto, gas
313 concentrations were converted into molar concentrations using the ideal gas law. From this, the
314 apparent O_2 consumption and apparent CO_2 production rates of the fruit were calculated using the
315 headspace volume of the jar and the volume of pear fruit cells. Finally, relative errors of the
316 apparent respiration rates $r_{O_{2,a}}$, $r_{CO_{2,a}}$ and RQ_a were calculated and compared.

317 # 3 Results

318 ## 3.1 Model fit to experimental data and respiration parameters

319 Figure 2 A – E depicts the experimentally determined gas concentrations of O_2 (blue circles) and
320 CO_2 (red circles) during the 1 d of flushing at 3.58 mol m^{-3} (8.0 kPa) O_2 and 3.58 mol m^{-3} (0.0
321 kPa) CO_2, followed by 10 d depletion of the respiration jars placed in a dark cool room at 0 °C.
322 Each figure represents the gas concentrations measured in a 1.7 L glass respiration jar containing
323 two 'Conference' pear fruit. During the 1 d period of flushing, the O_2 concentration and CO_2
324 concentration in all jars remained constant at 3.58 mol m^{-3} and 0.0 mol m^{-3}, respectively. After
325 flushing, when the jars were closed, the O_2 concentration in the headspace of the jars decreased
326 due to O_2 consumption by fruit respiration, while the CO_2 concentration in the headspace of the

jars increased by CO_2 production by fruit respiration. After 6.5 d, O_2 was completely depleted in all jars. From 7 d from the start of the depletion experiment onwards, although O_2 had been depleted, CO_2 gas concentrations still increased in all jars due to fermentative CO_2 production. Figure 2 A - E also shows the O_2 and CO_2 concentration inside the jars predicted by the model as a function of time during the experiment. For both O_2 and CO_2 gas concentrations in the headspace of the jars, the model fits the experimental data well. The estimated parameters are given in Table 1.

3.2 Gas concentrations inside fruit and evaluation of non-equilibrium assumption

Figure 3 A - E shows the average O_2 and CO_2 concentrations predicted by the model in the headspace of each 1.7 L jar, intercellular space, cell compartment, as well as the average concentration predicted by the model of HCO_3^- in the cell compartment. The lowest O_2 concentrations were found inside the cell compartment, due to consumption of O_2 by respiration. In the intercellular space the O_2 concentrations were found to be higher than in the cell compartment, but lower than in the ambient air in the jar surrounding the fruit, due the fruit skin resistance limiting O_2 gas exchange between fruit and air in the jar. During the period of 1 d of flushing, when the system was in steady-state, at 3.58 mol m^{-3} O_2 and 0.00 mol m^{-3} CO_2 in the headspace of the jars, O_2 concentrations of 3.05 mol m^{-3} and 0.146 mol m^{-3} were found in the intercellular space and cell compartment, respectively. Post-flushing, steady-state conditions were not satisfied anymore and O_2 concentrations started to decrease. After 6.5 d, O_2 concentrations in the jars, intercellular space and cell compartment, reached an average value of 0.399 mol m^{-3}, 0.166 mol m^{-3} and 0.003 mol m^{-3}, respectively. As the value of K_{m,O_2} in the respiration model is

equal to 0.003 mol m^{-3}, at this O_2 concentration fermentation rather than aerobic respiration will become the dominant energy pathway of the fruit. After 11 d, at the end of the experiment O_2 was completely depleted in the fruit cells (average concentration of 3.55×10^{-6} mol m^{-3}), while in the intercellular spacepace and headspace of the jars O_2 concentrations of 7.92×10^{-5} mol m^{-3} and 2.96×10^{-4} mol m^{-3} were found, respectively.

CO_2 concentrations were highest inside the cell compartment, as CO_2 is produced by respiration and is transported from cells to the environment. CO_2 concentrations in the intercellular spaces were lower than inside the cell compartment, but higher than the CO_2 concentrations in the jar, as the skin resistance of the fruit limits transport of CO_2 gas from the intercellular space to the environment. During the period of 1 d of flushing, when the system was in steady-state, at 3.58 mol m^{-3} O_2 and 0.00 mol m^{-3} CO_2 in the headspace of the jars, CO_2 concentrations of 0.331 mol m^{-3} and 0.509 mol m^{-3} were found in the intercellular space and cell compartment, respectively. Post-flushing, steady-state conditions were not longer satisfied, and CO_2 concentrations started to increase. After 6.5 d, O_2 concentrations in the cells approached the value of K_{m,O_2}, which is equal to 0.003 mol m^{-3}, again indicating a switch of aerobic respiration to fermentation. At this point, CO_2 concentrations of 4.41 mol m^{-3}, 2.88 mol m^{-3} and 2.79 mol m^{-3} were found in the cell compartment, intercellular space and headspace of the jars, respectively. After 10.86 d when the experiment was finished, CO_2 concentrations were 6.00 mol m^{-3}, 3.92 mol m^{-3} and 3.85 mol m^{-3} in the cell compartment, intercellular space and jar headspace, respectively.

Only very small concentrations of HCO_3^- were observed in the cell compartment. During the 1 d flushing period, when the system was in steady-state at 3.58 mol m^{-3} O_2 and 0.00 mol m^{-3} CO_2 in the headspace of the jars, the average HCO_3^- concentration in the cell was found to be 0.014 mol

371 m^{-3}. The HCO_3^- concentration in the cell compartment increased to a value of 0.0254 mol m^{-3} at
372 the end of the experiment during the depletion experiment.

373 To evaluate the assumption of non-equilibrium of the concentrations of O_2 and CO_2 in the
374 intercellular space and the cell compartment, gas concentrations in the intercellular space were
375 used to calculate the concentrations of O_2 and CO_2 in the cell compartment assuming equilibium
376 and using Henry's law. Figure 4 depicts the and O_2, CO_2 concentration in the cell compartment
377 assuming equilibrium and non-equilibrium, respectively, with the intercellular space. For both O_2
378 and CO_2 the simulations for equilibrium and non-equilibrium coincide, indicating the equilibrium
379 assumption holds. Therefore, the model proposed in this work for the intercellular space might
380 futher be simplified by lumping the cell compartment model with that of the intercellular space
381 (shown in Supplementary data S1):

382
$$\begin{cases} \left(\varepsilon + RTH_{O_2}\left(1-\varepsilon\right)\right)V_f \dfrac{dc_{O_2,g}}{dt} = -h_{O_2,s}A_s\left(c_{O_2,g} - c_{O_2,a}\right) + r_{O_2}\left(1-\varepsilon\right)V_f \\ \left(\varepsilon + RTH_{CO_2}\left(1-\varepsilon\right)\right)V_f \dfrac{dc_{CO_2,g}}{dt} = -h_{CO_2,s}A_s\left(c_{CO_2,g} - c_{CO_2,a}\right) + r_{CO_2}\left(1-\varepsilon\right)V_f + S_{CO_2}\left(1-\varepsilon\right)V_f \end{cases} \quad (16)$$

383 while the model for the first compartment, the storage headspace remains unchanged.

384 ## 3.3 Relation between cellular and headspace respiration rates

385 Figure 5 A illustrates the rates of O_2 consumption and CO_2 production in the fruit cells as a function
386 of the O_2 concentration in the jar headspace as predicted by the validated model, the simulated
387 rates of O_2 consumption and CO_2 productionin the headspace of the jars and the experimentally
388 measured rates of O_2 consumption and CO_2 production in the headspace of the jars. As the O_2
389 concentration in the jars decreases, the rate of O_2 consumption of the cells decreased starting from
390 2.72×10^{-5} mol m^{-3} s^{-1} at 3.12 mol m^{-3} O_2 in the jars to 0.0 mol m^{-3} s^{-1}, when the O_2 concentration

391 in the jars became 0.00 mol m^{-3}. The O_2 consumption rate in the headspace of the jars, slightly
392 underestimated, but closely corresponded to the O_2 consumption rate inside the fruit cells. The
393 simulated O_2 consumption rate apparent in the headspace of the jars started at 2.61×10^{-5} mol m^{-3}
394 s^{-1} at 3.12 mol m^{-3} O_2 in the jar and decreases until it reached a value of 0.00 mol m^{-3} s^{-1} when the
395 O_2 concentations in the jars became 0.00 mol m^{-3}. The simulated O_2 consumption rate apparent in
396 the headspace of the jars closely corresponded to the experimentally determined O_2 consumption
397 rate observed in the depletion experiment.

398 When the O_2 concentration in the jars decreased, the CO_2 production rate of the pear cells also
399 decreased from a starting value of 2.90×10^{-5} mol m^{-3} s^{-1}. Contrary to the O_2 consumption rate of
400 the pear cells, the CO_2 production rate of the pear cells did not decrease to zero as the O_2
401 concentration in the jars approached zero. Instead the CO_2 production rate of the cells reached a
402 value of 1.11×10^{-5} mol m^{-3} s^{-1} due to fermentation. Interestingly, the CO_2 production rate apparent
403 in the headspace of the jars, severely underestimated the actual CO_2 production rate of the pear
404 cells. The simulated CO_2 production rate apparent in the headspace of the jars starts at 1.78×10^{-5}
405 mol m^{-3} s^{-1} and reached a value of 6.56×10^{-6} mol m^{-3} s^{-1} at 0.00 mol m^{-3} O_2. Simulated CO_2
406 production rates apparent in the headpsace of the jars, closely corresponded to the experimentally
407 determined CO_2 production rates in the depletion experiment.

408 Figure 5 B depicts the relative difference of the simulated apparent O_2 consumption rate and CO_2
409 production rate in the jar headspace, relative to the simulated actual consumption rate in the fruit
410 cells as a function of the O_2 concentration in the jar headspace. At an O_2 concentration of 3.12 mol
411 m^{-3}, the value of the relative difference of the apparent O_2 consumption rate was 3.93 %. During
412 depletion, the relative difference of the apparent O_2 consumption rate slightly increased to a value
413 of 4.04 % at an O_2 concentration of 0.78 mol m^{-3} in the jar headspace. When the O_2 concentration

in the jars further decreased, the relative difference of the apparent O_2 consumption rate decreased to a value of 1.09 % when O_2 was completely depleted in the jars. For the relative difference of the CO_2 production rate apparent in the headspace of the jars, a value of 38.57 % was found at an O_2 concentration of 3.12 mol m^{-3}. The relative difference slightly increased to a value of 40.81 % at an O_2 concentration of 0.53 mol m^{-3}. From then on, the relative difference of the apparent CO_2 production rate increased to a value of 38.50 % at an O_2 concentration of 0.10 mol m^{-3}. When the O_2 concentration in the jar headspae further decreased to a value of 0.00 mol m^{-3}, the relative difference of the apparent CO_2 production rate increased again to a value of 40.89 %.

3.4 Relation between actual cellular and apparent headspace RQ values

The RQ in the pear fruit cells as a function of the headspace O_2 concentration in the jars is depicted in Figure 6 A. Under aerobic conditions, when no fermentation is triggered, the cellular RQ has a value of 1.00 at an O_2 concentration of 3.12 mol m^{-3}. As the O_2 concentration decreases and fermentation is triggered at an O_2 concentration of 0.399 mol m^{-3} in the jars, which corresponds to 0.003 mol m^{-3} in the cell compartment and which is the value of K_{m,O_2} in the respiration model, the RQ-value inside the pear fruit cells (RQ_{cell}) exponentially starts increasing up to values greater than 20.0 (not shown in Figure 6 A~~(a)~~), which is much larger than the model parameter RQ_{ox} (the RQ under aerobic conditions of 21 kPa O_2) used in the respiration model, which is equal to 1.0. Interestingly, the respiratory quotient as apparent in the headspace of the jars (RQ_a) underestimates the actual RQ-value in the pear cells. The experimentally determined RQ (RQ_{exp}) closely relates to the RQ in the jar headspace as predicted by the model (RQ_a). At the start of the simulation under aerobic conditions with an O_2 concentration of 3.12 mol m^{-3} s^{-1}, the apparent RQ has a value of 0.68, compared with 1.07 in the fruit cells. When the O_2 concentration was 0.11 mol

436 m^{-3} in the jars, an apparent RQ-value of 1.98 was observed. This value of the apparent RQ is very
437 close to the threshold RQ-value used in the RQ-DCA control algorithm for pome fruit presented
438 in Bessemans et al. (2016). However, at this moment when an apparent RQ-value of 1.98 is reached
439 in the jar headspace, the actual RQ in the pear cells was already equal to 3.16.

440 Figure 6 B shows the relative difference of the apparent respiratory quotient as if measured in the
441 headspace of the jars to the actual RQ-value of the fruit cells as function of the O_2 concentration.
442 An O_2 concentration of 3.12 mol m^{-3}, the relative difference of the apparent RQ as if measured in
443 the jar headspace at start of the simulation was 36.06 %. As the O_2 concentration in the jars
444 decreases, the relative difference of the apparent RQ increases to a value of 38.44 % at 0.46 mol
445 m^{-3} O_2. Then the relative difference of the apparent RQ decreases to a value of 37.35 % at 0.13
446 mol m^{-3} O_2. Finally the relative difference of the apparent RQ increases to a value of 40.69 % as
447 O_2 was completely depleted.

448 # 4 Discussion

449 ## 4.1 O_2 and CO_2 concentrations inside fruit cells and intercellular spaces

450 ## are in equilibrium

451 Based on the simulations, the gas concentrations in the cell compartment of 'Conference' pear
452 fruit under the assumption of equilibrium with the gas concentration in the intercellular space and
453 simulated using our non-equilibrium model, matched closely. The fruit cells may, thus, be
454 considered in equilibrium with the intercellular space. The model assuming non-equilibrium is a
455 more general model than the model using the equilibrium assumption. The results of the
456 comparative analysis of the non-equilibrium model and the model using the equilibrium

assumption have shown that the equilibrium assumption holds and that therefore the non-equilibrium model can be simplified using the equilibrium assumption as demonstrated in Supplementary material S1.This equilibrium approach has previously been used by Ho et al. (2010, 2013, 2018), where gas concentrations in the cell compartment of apple and pear fruit were calculated from the gas concentrations in the intercellular space using a partition coefficient based on Henry's law. Our results confirm that gas concentrations may indeed be regarded in equilibrium with the intercellular space.

4.2 Respiration rates observed in headspace underestimate respiration

In Ssection 3.3, we showed that apparent O_2 consumption rates and CO_2 production rates, measured in storage headspace, underestimate the actual O_2 consumption and CO_2 production rates in the fruit cortex cells. The relative error of the O_2 consumption rate was found to be maximally 4 %, while the relative error of the CO_2 consumption rates was found to he as high as 41 %. The difference in rate of change of the gas concentrations of O_2 and CO_2 in the headspace and in the fruit cells is due the solubility of O_2 and CO_2 in the cell compartment (Saltveit 2019) and the cell and fruit skin resistances limiting gas exchange between fruit and storage environment. Due to its high solubility, CO_2 molecules produced by respiration, dissolve in the cell compartment, preventing them to be transported out of the cell compartment and into to the storage headspace. Therefore, the concentration of CO_2 gas in the storage headspace changes more slowly than the concentration of CO_2 in the intracellular compartment. This is in accordance to previous calculations conducted by Saltveit (2019), who found the solubility of CO_2 in the cellular liquid of apple fruit to result in underestimation of the CO_2 production rate as observed in the headspace of a static respirometer by 17 %. The explanation for the error found in CO_2 production rate by Saltveit (2019) to be only half the error found in this work, lies in the fruit-to-free-volume-ratio in

480 the respirometer. In the calculations of Saltveit (2019), a ratio of 0.22 was used, while in our work
481 an average ratio of 0.45 was used, resulting in an error twice as large.

482 Although CO_2 concentrations in the cellular liquid are high, those of HCO_3^- remain low as H_2CO_3
483 is a weak acid (pKa = 6.35) and the cellular pH is equal to 5.0. Furthermore, the cell and fruit skin
484 resistance will prevent the CO_2 that has already moved from the cell compartment to the
485 intercellular space to diffuse out of the fruit, leading to an underestimation of cellular CO_2
486 production based on storage headspace measurements. O_2 consumption by respiration creates
487 lower O_2 concentrations in the cell compartment and intercellular space than in the storage
488 headspace. Due to its solubility in the cell compartment, O_2 dissolves in the cell compartment,
489 although it is not instantaneously consumed by fruit respiration. Theoretically this would lead to
490 an overestimation of the actual O_2 consumption rate by the apparent O_2 consumption rate. Because
491 the solubility of O_2 in the cell compartment is much smaller compared to that of CO_2 (Henry
492 constants of 2.11×10^{-5} mol m^{-3} Pa^{-1} and 6.4×10^{-4} mol m^{-3} Pa^{-1} for O_2 and CO_2, respectively (Lide
493 1999), this effect is rather small. As cell permeabilities are comparable for O_2 and CO_2 (3.37×10^{-5} m s^{-1} and 2.77×10^{-5} m s^{-1}, respectively), it is the low permeability of the pear fruit skin for O_2
495 compared to CO_2 (1.86×10^{-7} m s^{-1} and 5.06×10^{-7} m s^{-1}, respectively (Table 1)) that results in a
496 delay of O_2 moving from the storage headspace and, therefore, leading to an underestimation of
497 the actual cellular O_2 consumption rate by the apparent O_2 consumption rate measured in storage
498 headspace. Although this work focusses on static respirometers, as is the case in commercial
499 storage environment of pome fruit, it is worth noting that flow-through techniques and techniques
500 using permeable packages for respiration determination avoid the problem of underestimating
501 respiration rates as steady-state conditions are satisfied during respiration measurement (Fidler and
502 North, 1967; Beaudry 1993).

4.3 Apparent RQ values in headspace underestimates cellular RQ

From the simulation results it is clear that apparent RQ values measured in storage headspace, underestimate actual RQ-values in 'Conference' pear fruit cells. The idea of using RQ-values measured in storage headspace as a bio response to detect low O_2 stress has been around long time already (Jozwiak and Blanpied, 1993). Until now, it was assumed that fruit stored in CA were in steady-state with the storage environment during measurement of RQ based on changes in concentrations of O_2 and CO_2 in storage headspace. We show that the steady-state assumption does not hold from the moment that flushing or actions of a CA control system stop and gas concentrations in the storage atmosphere start changing,. Under steady-state, it is assumed that all CO_2 produced by respiration immediately diffuses out of the fruit and that the amount of O_2 consumed by respiration immediately diffuses from the storage environment in the fruit. This assumption clearly does not hold, as demonstrated by the large relative errors of apparent O_2 consumption and CO_2 production rates up to 4.4 % and 40.89 % respectively. Underestimation of the actual RQ value of cells of fruit stored under RQ-based DCA storage implies the risk of storing fruit at O_2 concentrations which are far below the ACP, leading to the development of flavor and storage disorders (Franck et al., 2007). In this work we showed that at a headspace O_2 concentration of 0.11 mol m^{-3} (0.25 kPa), an apparent RQ-value of 1.98 was observed in headspace, while the cellular RQ of the 'Conference' fruit was already 3.16. This finding of underestimation of cellular RQ based on storage headspace RQ calculations confirms observations done by Delele et al. (2019), who found RQ values of 3.04 in the headspace of a storage container of 'Conference' pear fruit, while cellular RQ was already equal to 5.08 (Delele et al., 2019). The underestimation of cellular RQ by headspace observations may explain why RQ-based DCA storage of pear fruit has, so far, not been reported in literature. Also, this may explain why 'Galaxy' apples stored under

RQ-based dynamic controlled atmosphere storage at RQ-levels of 1.3 and 1.5, showed an increased abundance of aroma componds related to low O_2 stress, which are not observed under regular CA storage as reported by Thewes et al. (20170. The relative error of the RQ observed in the storage headspace of about 40 % remains quite constant when the O_2 and CO_2 concentrations in the storage space decrease and increase, respectively. This is because the relative errors of the r_{O2} and r_{CO2} remain more or less constant. A possible explanation for this is that the solubility of O_2 and CO_2 into the cellular liquid does not change with decreasing O_2 concentrations or increasing CO_2 concentrations. Therefore, the same fraction of e.g. CO_2 produced is dissolved and not observed in the headspace independently of the respiration rate. The relative error of the RQ observed in the storage headspace of 40 % is the relative error of what is observed as RQ in the jar headspace given the respiration rates and RQ in the cells. The error calculation does not include any model error. As the models used try to capture all relevant physical and biochemical processes, they are assumed to be correct. Probably the models are not perfect, so depending on the errors of the different models involved, the true error of the headspace RQ model can slightly deviate from 40 %.

Often, the RQ-breakpoint is experimentally determined based measurement conducted in the headspace of a static respirometer. Our results demonstrate that there is a underestimation of the RQ in the fruit cells by the RQ-values observed in the storage headspace. As a consequence, detection of low O_2 stress will be too late, as the RQ-breakpoint in the cells occurs much earlier than it can be observed in the storage headspace. As it is not possible to measure the respiration rate inside the fruit cells, our modelling approach provides a useful alternative to determine the RQ of the fruit cells based on storage headspace measurements.

548 Based on the results presented in this work, existing RQ-based DCA control systems should be
549 adapted and lower threshold values of apparent RQ measured in storage headspace should be used.
550 In a next step, the model can be used for development of model-based control system that combines
551 the in this work developed fruit-enviroment gas exchange model with a leakage model of the
552 storage environment (Bessemans et al, 2018) and measured respiration rates to obtain more reliable
553 RQ estimates and improve RQ-based DCA storage in practice.

554 # 5 Conclusions

555 A three-compartment non-equilibrium gas transport model of 'Conference' pear fruit under CA
556 storage conditions was developed. A respiration model based on Michaelis-Menten respiration
557 kinetics without inhibition of respiration by CO_2 and incorporating down-regulation of respiration
558 was used. Conversion of CO_2 dissolved in the cell compartment to HCO_3^- at a constant pH of 5.00
559 was included. The model was validated based on experimental data of pear fruit during a complete
560 depletion experiment starting from 3.58 mol m^{-3} O_2 and 0.00 mol m^{-3} CO_2. Model predictions
561 match experimental observations well. Gas concentrations in the cell compartment were found to
562 be in equilibrium with the gas concentrations in the intercellular space. The model was used to
563 calculate apparent respiration rates and RQ as if measured in the storage headspace. It was found
564 that apparent respiration rates and RQ, calculated based on headspace measurements,
565 underestimate the actual respiration rate and respiratory quotient in the fruit cells more than 40 %.

566 # Acknowledgements

567 Financial support by the Institute Flanders Innovation & Entrepreneurship (VLAIO, innovation
568 mandate of N. Bessemans, HBC.2017.0549) and KU Leuven (project C16/16/002) is gratefully
569 acknowledged.

6 Tables

Table 1: Model parameters of the gas exchange model.

Model parameter	*Symbol*	*Value*	*Units*	*Source*
Fruit-environment gas exchange				
Tissue porosity	ε	0.57×10^{-1}	$m^3\ m^{-3}$	Herremans et al 2015
Diffusivity of O_2 in the fruit skin	$D_{O_2,s}$	1.86×10^{-10}	$m^2\ s^{-1}$	Ho et al 2010
Diffusivity of CO_2 in the fruit skin	$D_{CO_2,s}$	5.06×10^{-10}	$m^2\ s^{-1}$	Ho et al 2010
Thickness of the fruit skin	δ_s	1.00×10^{-3}	m	Ho et al 2008
Cell-pores gas exchange				
Specific surface pear tissue	A_{cortex}	1.56×10^{3}	$m^2\ m^{-3}$	Micro-CT
Thickness of the cell walls	δ_{cw}	7.30×10^{-7}	m	Ho et al 2009
Diffusivity of O_2 in the cell wall	$D_{O_2,cw}$	4.25×10^{-9}	$m^2\ s^{-1}$	Ho et al 2009
Diffusivity of CO_2 in the cell wall	$D_{CO_2,cw}$	5.23×10^{-9}	$m^2\ s^{-1}$	Ho et al 2009
Thickness of the cell membranes	δ_{cm}	8.00×10^{-9}	m	Ho et al 2009
Diffusivity of O_2 in cell membrane	$D_{O_2,cm}$	2.91×10^{-9}	$m^2\ s^{-1}$	Ho et al 2009
Diffusivity of CO_2 in cell membrane	$D_{CO_2,cm}$	2.80×10^{-11}	$m^2\ s^{-1}$	Ho et al 2009
Henry constant of O_2	H_{O_2}	2.11×10^{-5}	$mol\ m^{-3}\ Pa^{-1}$	Ho et al 2009
Henry constant of CO_2	H_{CO_2}	6.70×10^{-4}	$mol\ m^{-3}\ Pa^{-1}$	Ho et al 2009
Cell equivalent spherical radius	R_{cell}	0.80×10^{-4}	m	Herremans et al 2015

Table 2: Respiration model parameters

Model parameter	*Symbol*	*Value*	*Standard deviation*	*Units*	*Source*
Initial maximal O_2 consumption rate at 3.58 [mol m^{-3}] O_2	V_{m,O_2}	3.08×10^{-5}	5.81×10^{-10}	mol $m^{-3}s^{-1}$	Estimated
Maximal fermentative CO_2 production rate	V_{m,f,CO_2}	1.11×10^{-5}	3.00×10^{-10}	mol m^{-3} s^{-1}	Estimated
MM constant O_2 consumption rate of pear protoplasts	K_{m,O_2}	3.00×10^{-3}		mol m^{-3}	Lammertyn et al 2000
MM constant fermentative CO_2 production rate	K_{m,f,O_2}	2.50×10^{-2}	5.43×10^{-7}	mol m^{-3}	Estimated
Respiratory quotient under aerobic conditions	RQ_{ox}	1.0		[-]	Ho et al., 2011
Response rate of maximal O_2 consumption rate to changing O_2	k_d	4.72×10^{-6}	2.52×10^{-6}	s^{-1}	Estimated
Sensitivity of maximal O_2 consumption rate to O_2	K_H	1.06	3.11×10^{-6}	mol^2 m^{-6}	Estimated
O_2 consumption rate in presence of O_2	$V_{r,2}$	10.29×10^{-5}	2.52×10^{-9}	mol m^{-3} s^{-1}	Estimated
Basal maximal O_2 consumption rate	$V_{r,1}$	1.13×10^{-5}	1.40×10^{-10}	mol m^{-3} s^{-1}	Estimated

Table 3: Parameters of the CO_2 conversion model

Model parameter	*Symbol*	*Value*	*Units*	*Source*
H_2CO_3 acid dissociation constant	K	0.00025	mol L^{-1}	Ho et al 2009
CO_2 hydration rate constant	k_1	0.039	s^{-1}	Ho et al 2009
HCO_2 dehydration constant	k_2	23	s^{-1}	Ho et al 2009

7 Figures

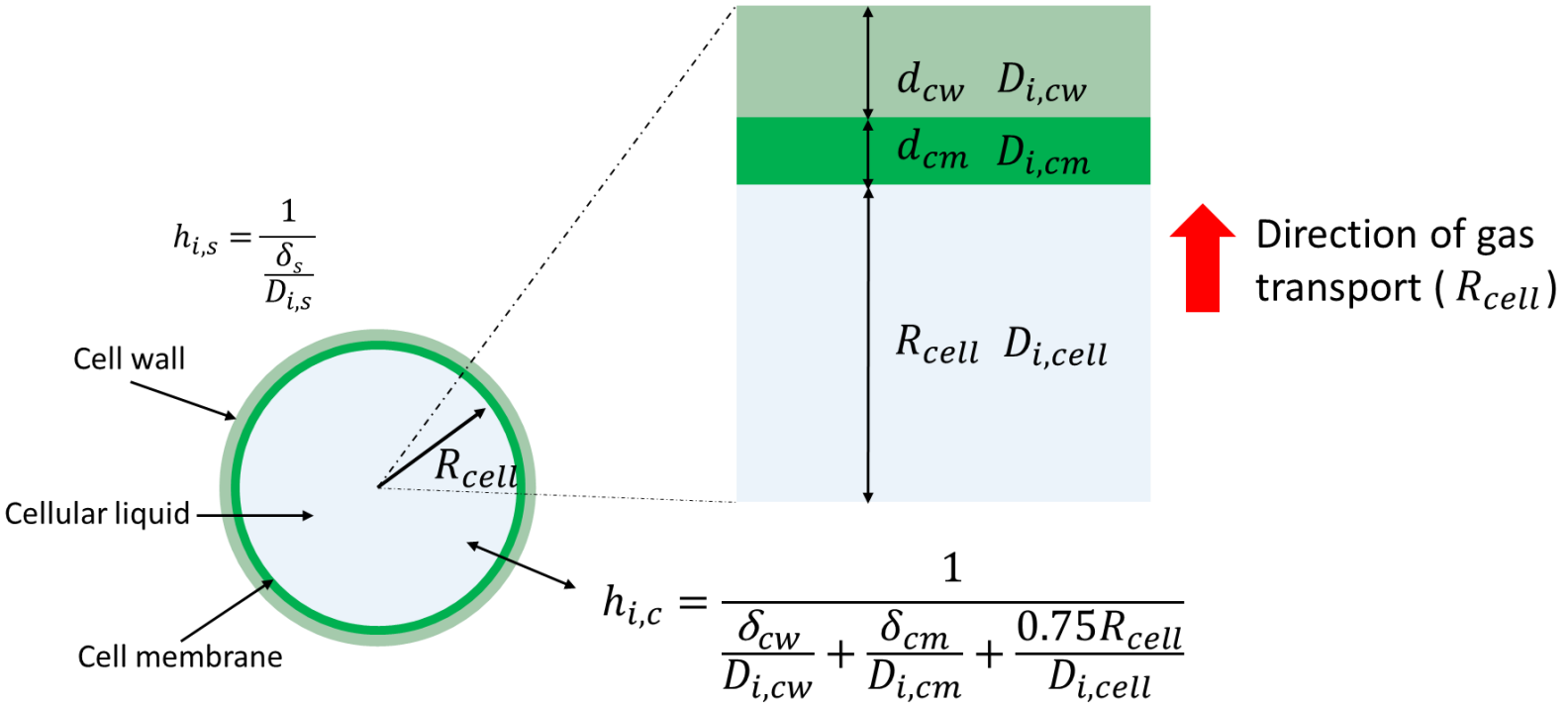

Figure 1: Schematic overview of the main resistances in the gas exchange model of fruit and storage environment. (a) Fruit skin resistance limiting gas exchange between fruit and storage environment. (b) Cell resistance limiting gas exchange between fruit cells and intercellular porres in the fruit cortical tissue. The cell resistance consists of the resistanes of the cell wall, cell membrane and cell compartment in series. As cells are assumed to be spherical, only radial transport is considered.

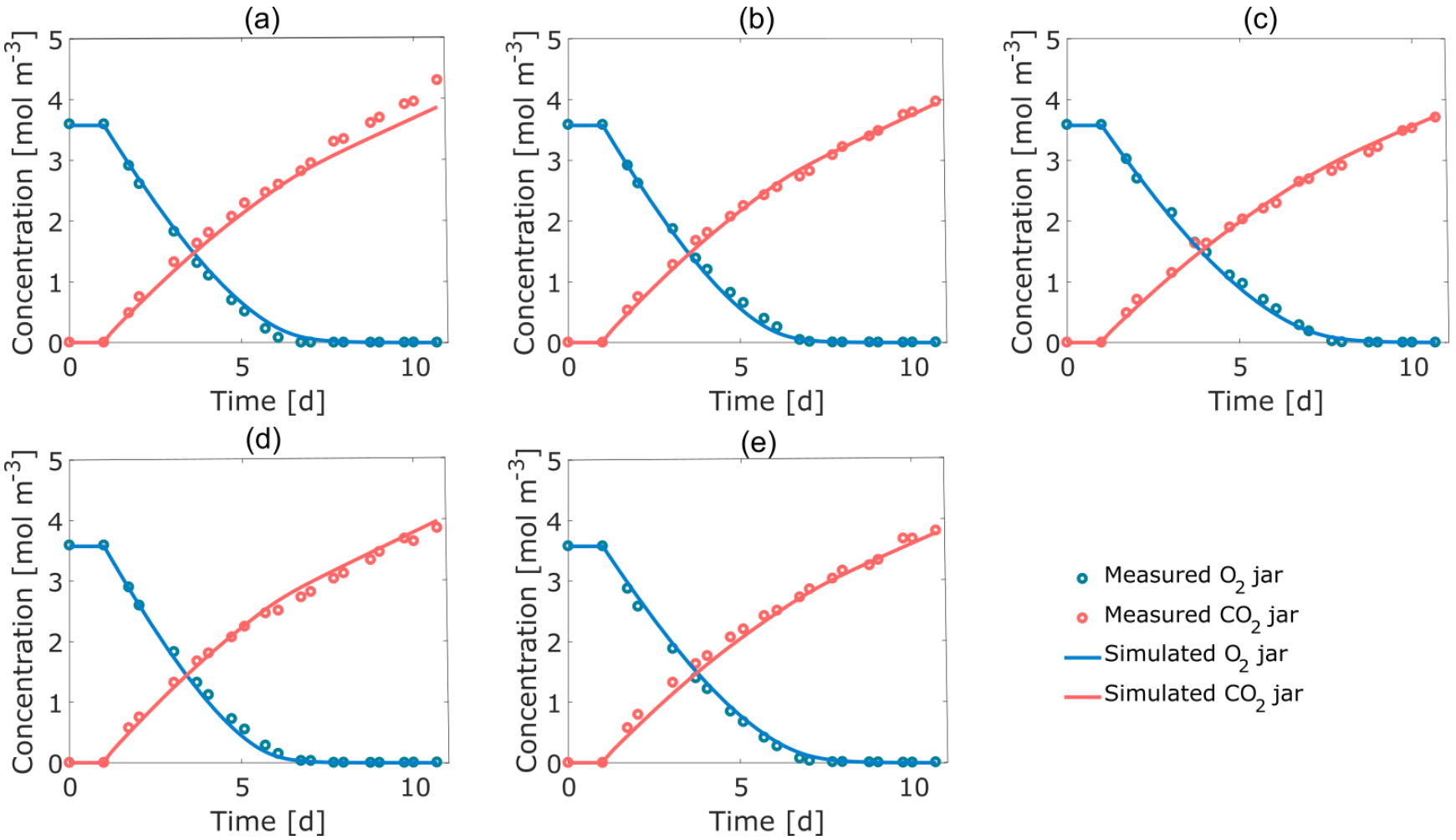

Figure 2 (a) - (e): Experimentally determined O_2 (blue circles) and CO_2 (red circles) concentrations and simulated O_2 (full blue line) and CO_2 (full red line) concentrations during the 1 d of flushing at 8.0 kPa O_2 and 0.0 kPa CO_2 followed by 10 d depletion experiment with respiration jars. Each figure (a) – (e) represents the gas concentrations measured in a 1.7 L glass respiration jar containing 2

'Conference' pear fruit. The ratio of fruit volume to headspace volume in the jar was 0.45 ± 0.036. For interpretation of the references to color in this figure legend, the reader is referred to the web version of this article.

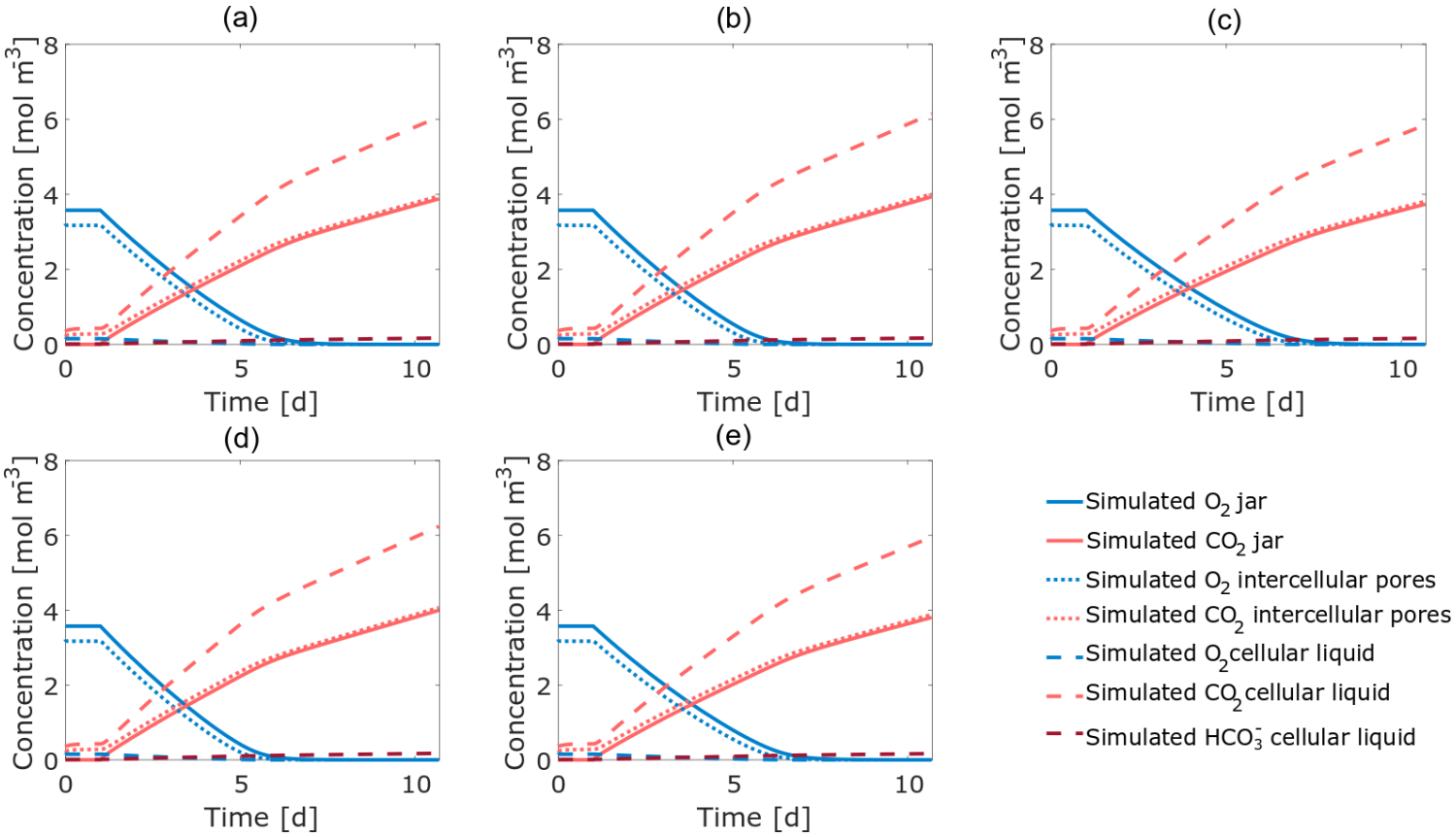

Figure 3 (a) – (e): Concentrations of O_2 in the headspace of the jar (full blue line), intercellular space (dotted blue line), cell compartment (dashed blue lines) and concentrations of CO_2 in the headspace of the jars (full red line), intercellular space (dotted red line), cell

compartment (dashed red line) and bicarbonate concentration in the cell compartment (dashed maroon line). Each figure (a) - (e) represents the gas concentrations measured in a 1.7 L glass respiration jar containing 2 'Conference' pear fruit. The ratio of fruit-to-headspace volume was 0.45 ± 0.036. For interpretation of the references to color in this figure legend, the reader is referred to the web version of this article.

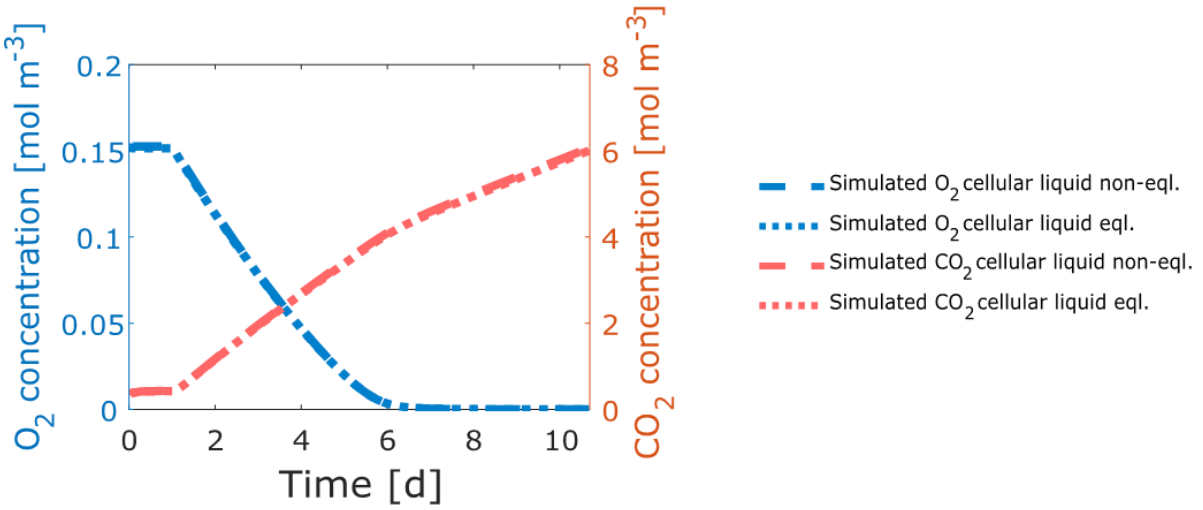

Figure 4: Concentrations of O_2 (dashed blue line) and CO_2 (dashed red line) in the cell compartment as predicted by the non-equilibrium model and concentrations of O_2 (dotted blue line) and CO_2 (dotted red line) in the cell compartment assuming equilibrium and calculated from the gas concentrations in the intercellular space calculated using Henry's law. The graph represents the gas concentrations measured

the first 1.7 L glass respiration jar containing 2 ‘Conference’ pear fruit. For interpretation of the references to color in this figure legend, the reader is referred to the web version of this article.

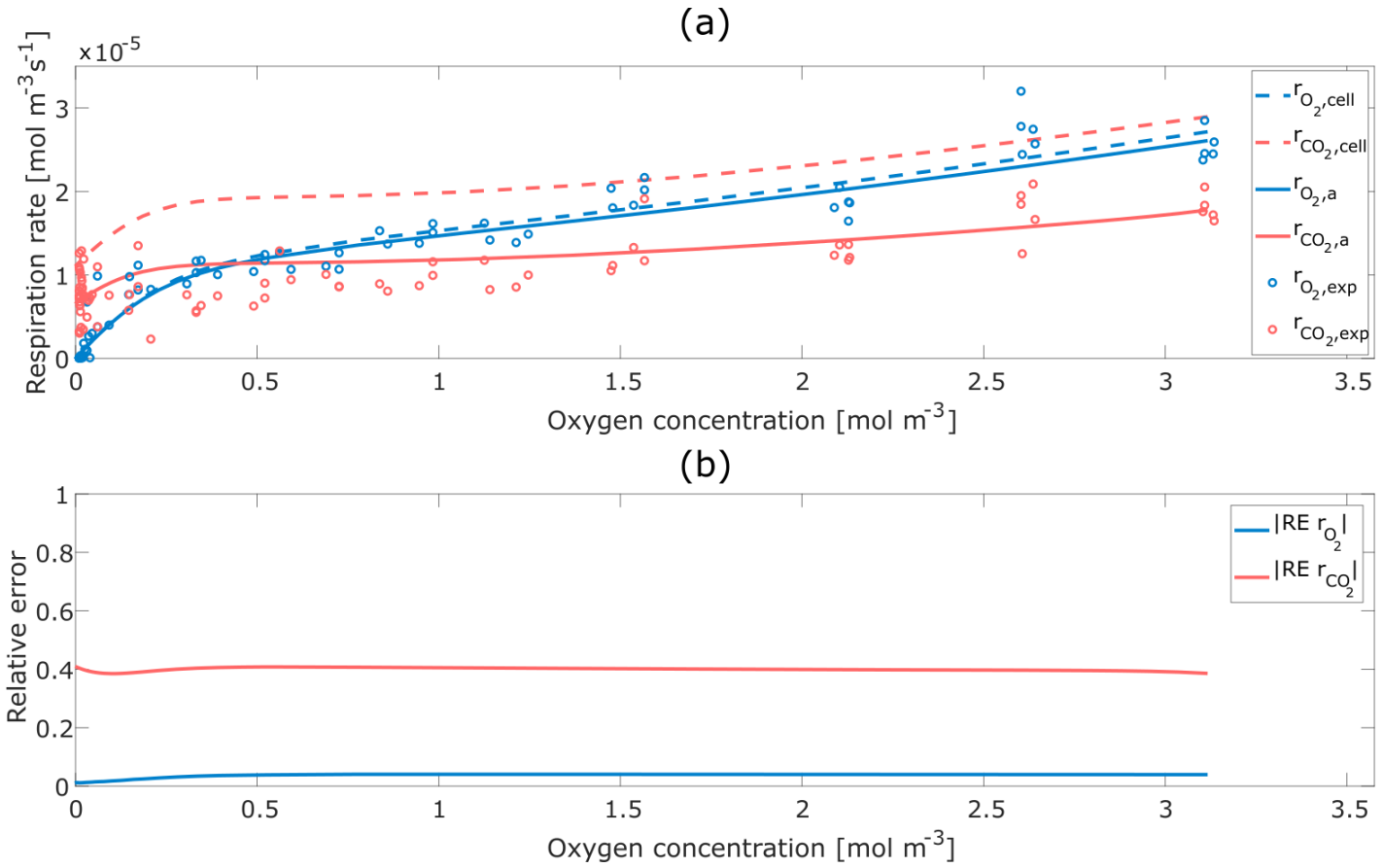

Figure 5 (a): Measured O_2 consumption rate (blue circles), measured CO_2 production rate (red circles) and simulated O_2 consumption rate (full blue line), simulated CO_2 production rate (full red line) as a function of O_2 concentration during the depletion experiment using 1.7 L respiration jars containing 2 fruit each. (b) relative error of the the simulated apparent O_2 consumption rate and CO_2 production rate in the jar headspace to the simulated actual consumption rate in the fruit cells, indicated by a full blue line and a full red line,

respectively. Simulations were conducted using a fruit-to-headspace volume of 0.45 ± 0.036. For interpretation of the references to color in this figure legend, the reader is referred to the web version of this article.

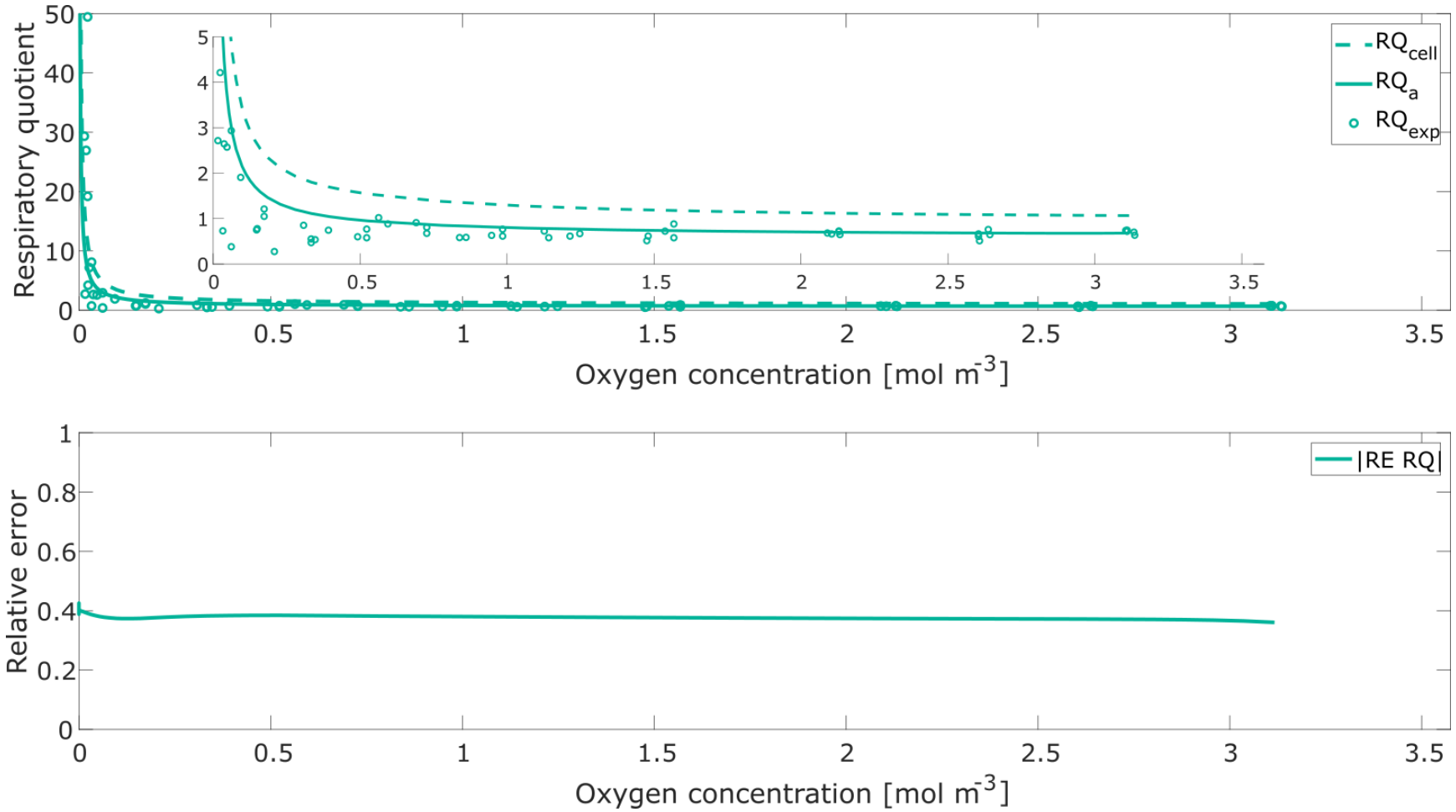

Figure 6: (a) Measured apparent respiratory quotient values (green circles), simulated values of the respiratory quotient in 'Conference' pear fruit cells (dashed green line) and simulated values of the respiratory quotient in headspace (full green line) as function of O_2 concentration during the depletion experiment using 1.7 L respiration jars containing 2 fruit each. (b) Relative error of the the simulated

apparent respiratory quotient in the jar headspace compared to the simulated respiratory quotient in the fruit cell. For interpretation of the references to color in this figure legend, the reader is referred to the web version of this article.

Literature cited

Andrich G., Zinnai A., Venturi E., Silvestri S., Fiorentini R., 2006. A tentative mathematical model to describe the evolution of the aerobic and anaerobic respiration rates of golden delicious apples with temperature, PO_2 and PCO_2. Italian Journal of Food Science. 18, 3–19

Beaudry, R. M. 1993. Effect of carbon dioxide partial pressure on blueberry fruit respiration and respiratory quotient. Postharvest Biology and Technology, 3, 249–258

Bessemans, N., Verboven, P., Verlinden, B.E., Nicolaï, B.M., 2018. Model based leak correction of real-time RQ measurement for dynamic controlled atmosphere storage. Postharvest Biol. Technol. 136, 31–41. doi:10.1016/j.postharvbio.2017.09.011

Bessemans, N., Verboven, P., Verlinden, B.E., Nicolaï, B.M., 2016. A novel type of dynamic controlled atmosphere storage based on the respiratory quotient (RQ-DCA). Postharvest Biol. Technol. 115, 91–102. doi:10.1016/j.postharvbio.2015.12.019

Boersig, M.R., Kader, A.A., Romani, R.J., 1988. Aerobic–anaerobic respiratory transition in pear fruit and cultured pear fruit cells. J. Am. Soc. Hortic. Sci. 113, 869–873.

Both, V., Rodrigo, F., Brackmann, A., Oliveira, R. De, Freitas, D. De, Wagner, R., 2017. Effects of dynamic controlled atmosphere by respiratory quotient on some quality parameters and volatile profile of 'Royal Gala' apple after long-term storage. Food Chem. 215, 483–492. doi:10.1016/j.foodchem.2016.08.009

Brackmann, A., 2015. Control apparatus for controlled atmosphere cells for storing perishable items. U.S. Patent, n. US2015/0257401 A1.

Burg, S.P. and Burg, E.A., 1965. Gas exchanges in fruits. Physiol. Plant. 18, 870–884.

Cameron A.C., Beaudry, R.m., banks, N.H., Yelanich, M.V., 1994. Modified-Atmosphere Packaging Of Blueberry Fruit - Modeling respiration and package oxygen partial pressures as a Function of temperature. J. Am. Soc. Hortic.Sci. 119 (3), 534-539.

Delele, M.A., Bessemans, N., Gruyters, W., Rogge, S., Janssen, S., Verlinden, B.E., Smeets, B., Ramon, H., Verboven, P., Nicolaï, B.M., 2019. Spatial distribution of gas concentrations and RQ in a controlled atmosphere storage container with pear fruit in very low oxygen conditions. Postharvest Biol. Technol. 156, 110903. https://doi.org/10.1016/j.postharvbio.2019.05.004

DeLong, J.M., Prange, R.K., Leyte, J.C., Harrison, P. A., 2004. A new technology that determines low-O_2 thresholds in controlled-atmosphere-stored apples. Horttechnology 14, 262–266.

Dilley, D.R., 2010. Controlled atmosphere storage - chronology and technology, in: Acta Horticulturae 857, 493–502

Fidler, J. C., & North, C. J., 1967. The effect of conditions of storage on the respiration of apples. I. The effects of temperature and concentrations of carbon dioxide and oxygen on the production of carbon dioxide and uptake of oxygen. Journal of Horticultural Science, 42, 189–206

Fonseca, S.C., Oliveira, F.A., Brecht, J.K., 2002. Modelling respiration rate of fresh fruits and vegetables for modified atmosphere packages: a review. J. Food Eng. 52, 99–119. doi:10.1016/S0260-8774(01)00106-6

Franck, C., Lammertyn, J., Ho, Q.T., Verboven, P., Verlinden, B., Nicolaï, B.M., 2007. Browning disorders in pear fruit. Postharvest Biol. Technol. 43, 1–13. doi:10.1016/j.postharvbio.2006.08.008

Gasser, F., Eppler, T., Naunheim, W., Gabioud, S., Bozzi Nising, A., 2010. Dynamic CA storage of apples: Monitoring of the critical O_2 concentration and adjustment of optimum conditions during O_2 reduction. Acta Hortic. 876, 39–46. doi:10.17660/ActaHortic.2010.876.3

Gran, C.D., Beaudry, R.M., 1993. Determination of the low O_2 limit for several commercial apple cultivars by respiratory quotient breakpoint. Postharvest Biol. Technol. 3, 259–267. doi:10.1016/0925-5214(93)90061-7

Gupta, A., Teja, A., Chai, X., Zhu, J., 2000. Henry's constants of n-alkanols (methanol through n-hexanol) in water at temperatures between 40 °C and 90 °C. Fluid Phase Equilib. 170, 183–192. doi:10.1016/S0378-3812(00)00350-2

Herremans, E., Verboven, P., Hertog, M.L.A.T.M., Cantre, D., 2015a. Spatial development of transport structures in apple (*Malus* ×*domestica* Borkh .) fruit. Front Plant Sci. 6, 679. doi:10.3389/fpls.2015.00679

Herremans, E., Verboven, P., Verlinden, B.E., Cantre, D., Abera, M., Wevers, M., Nicolaï, B.M., 2015b. Automatic analysis of the 3-D microstructure of fruit parenchyma tissue using X-ray micro-CT explains differences in aeration. BMC Plant Biol. 1–14. doi:10.1186/s12870-015-0650-y

Hertog, M .L. A. T. M., Peppelenbos, H. W., Evelo, R. G., Tijskens, L.M.M., 1998. A dynamic and generic model of gas exchange of respiring produce : the effects of O_2 , CO_2 and temperature. Postharvest Biol. Technol. 14, 335–349.

Hertog, M.L.A.T.M., Verlinden, B.E., Lammertyn, J., Nicolaï, B.M., 2007. OptiPa, an essential primer to develop models in the postharvest area, Computers and Electronics in Agriculture. doi:10.1016/j.compag.2007.02.001

Ho, Q.T., Hertog, M.L.A.T.M., Verboven, P., Ambaw, A., Rogge, S., Verlinden, B.E., Nicolaï, B.M., 2018. Down-regulation of respiration in pear fruit depends on temperature 69, 2049–2060. doi:10.1093/jxb/ery031

Ho, Q.T., Verboven, P., Verlinden, B.E., Schenk, A., Delele, M. a., Rolletschek, H., Vercammen, J., Nicolaï, B.M., 2010. Genotype effects on internal gas gradients in apple fruit. J. Exp. Bot. 61, 2745–2755. doi:10.1093/jxb/erq108

Ho, Q.T., Verboven P., Mebatsion, K.H., Verlinden, B.E., Vandewalle, S., Nicolaï, B.M., 2009. Microscale mechanisms of gas exchange in fruit tissue. New Phytologist 182, 163-174. doi:10.1111/j.1469-8137.2008.02732.x.

Ho, Q.T., Verboven, P., Verlinden, B.E., Herremans, E., Wevers, M., Carmeliet, J., Nicolaı, B.M., 2011. A three-dimensional multiscale model for gas exchange 155, 1158–1168. doi:10.1104/pp.110.169391

Ho, Q.T., Verboven, P., Verlinden, B.E., Schenk, A., Nicolaï, B.M., 2013. Controlled atmosphere storage may lead to local ATP deficiency in apple. Postharvest Biol. Technol. 78, 103–112. doi:10.1016/j.postharvbio.2012.12.014

Hoehn, E., Prange, R.K., Vigneault, C., 2009. Storage technology and applications, in modified and controlled atmospheres for the storage, transportation and packaging of horticultural commodities. CRC press, Boca Raton.

Jozwiak, Z.B., Blanpied, G.D., 1993. A study of some orchard and storage factors that influence the O_2 threshold for ethanol accumulation in stored apples., in: In: CA ’93. Proc. 6thIntl.Controlled Atmosphere Research Conference, Cornell Univ., Ithaca, NY. Northeast Reg. Agric. Eng. Service, Ithaca, NY, USA. pp. 45–53.

Kader, A. A., 1997. A summary of CA requirements and recommendations for fruits other than apples and pears. Proc. 7th Int. Control. Atmos. Res. Conf. Vol. 3, Davis, CA, USA, 1-34.

Knee, M., Hatfield, S.G.S., 1976. A comparison of methods for measuring the volatile components of apple fruits. Food Sci. Technol. 11, 485–493.

Kurkdjian A, Leguay J, Guern J. 1978. Measurement of intracellular pH and aspects of its control in higher plant cells cultivated in liquid medium. Respiration Physiology33: 75–89.

Lammertyn, J., 2001. A respiration-diffusion model to study core breakdown in Conference pears. PhD dissertation. Katholieke Universiteit Leuven. Belgium.

Lammertyn, J.., Franck, C., Verlinden, B.E., Nicolaï, B.M., 2001. Comparative study of the O_2, CO_2 and temperature effect on respiration between 'Conference' pear cell protoplasts in suspension and intact pears. J. Exp. Bot. 52, 1769–1777. doi:10.1093/jexbot/52.362.1769

Lammertyn, J., Scheerlinck, N., Jancsók, P., Verlinden, B.., Nicolaıi, B., 2003. A respiration–diffusion model for “Conference” pears I: model development and validation. Postharvest Biol. Technol. 30, 29–42. doi:10.1016/S0925-5214(03)00061-9

Lide DR. 1999. Handbook of Chemistry and Physics. New York, NY, USA: CRC Press.

Nobel PS. 1991. Physicochemical and environmental plant physiology. London, UK: Academic Press Inc., 1– 46.

Ogren, E., 1990. Evaluation of chlorophyll fluorescence as a probe for drought stress in willow leaves. Plant Physiol. 93, 1280–1285. doi:10.1104/pp.93.4.1280

Oliveira, R. De, Brackmann, A., Mallmann, L., Rodrigo, F., Eliseu, E., Ludwig, V., Roberto, M., Berghetti, P., 2018. Interaction of 1-methylcyclopropene , temperature and dynamic controlled atmosphere by respiratory quotient on 'Galaxy' apples storage. Food Packag. Shelf Life 1–11. doi:10.1016/j.fpsl.2018.07.004

Peppelenbos, H.W., 2003. How to control the atmosphere? Postharvest Biol. Technol. 27, 1–2. doi:10.1016/S0925-5214(02)00192-8

Peppelenbos H.W., Van't Leven, J., 1996. Evaluation of four types of inhibition for modelling the influence of CO_2 on O_2 consumption of fruits and vegetables. Postharvest Biol. Technol. 7, 27–40.

Pesis, E., Dvir, O., Feygenberg, O., Arie, R. Ben, Ackerman, M., Lichter, A., 2002. Production of acetaldehyde and ethanol during maturation and modified atmosphere storage of litchi fruit. Postharvest Biol. Technol. 26, 157–165. doi:10.1016/S0925-5214(02)00024-8

Prange, R.K., DeLong, J.M., Leyte, J.C., Harrison, P.A., 2002. O_2 concentration affects chlorophyll fluorescence in chlorophyll-containing fruit. Postharvest Biol. Technol. 24, 201–205. doi:10.1016/S0925-5214(01)00188-0

Renault, Y., Houal, L., Jaquemin, G., Chambroy, G., 1994. Gas exchange in modified atmosphere packaging- 2 experimental results with strawberries, J. Food Sci. Technol. 29, 379-394.

Roberts J.K.M., Wemmer D., Ray, P.M., Jardetzky, O. 1982. Regulation of cytoplasmic and

vacuolar pH in maize root tips under different experimental conditions. Plant Physiology 69: 1344 –1347.

Rosenberg, R.M., Peticolas, W.L., 2004. Henry ’s Law : A retrospective 81, 1647–1652.

Saltveit, M.E., 2003. Is it possible to find an optimal controlled atmosphere? Postharvest Biol. Technol. 27, 3–13. doi:10.1016/S0925-5214(02)00184-9

Saltveit, M.E., 2019. Chapter 4: Respiratory metabolism. In: Yahia, E. (Editor), Postharvest Physiology and Biochemistry of Fruit and Vegetables. Woodhead Publishing, Cambridge, p 73-91.

Schaefer, J.C., Bishop, D.J. 2014. Dynamic control system and method for controlled atmosphere roon. US patent. Patent number: US8739694 B2.

Schouten, S.O.P., Prange, R.K., Verschoor, J., Lammers, T.R. and Oosterhaven, J., 1997. Improvement of quality of 'Elstar' apples by dynamic control of ULO conditions. Proc. 7th CA Res. Conf., Postharvest Hortic. Ser. 16, 71–78.

Smith, R. E., Bennett, A. H. (1965). Mass–average temperature of fruits and vegetables during transient cooling. Transactions of the ASAE, 8, 249–252.

Smith F.A., Raven J.A. 1979. Intracellular pH and its regulation. Annual Review of Plant Physiology 30: 289–311.

Thewes, F.R., Brackmann, A., Anese, R., Ludwig, V., Schultz, E.E., dos Santos, L.F., Wendt, L.M. 2017. **Effect of dynamic controlled atmosphere monitored by respiratory quotient and 1-methylcyclopropene on the metabolism and quality of 'Galaxy' apple harvested at three maturity stages**. Food Chem., 222, pp. 84-93, doi:10.1016/j.foodchem.2016.12.009

Veltman, R.., Verschoor, J.., van Dugteren, J.H.R., 2003. Dynamic control system (DCS) for apples (*Malus x domestica* Borkh. cv 'Elstar'): optimal quality through storage based on product response. Postharvest Biol. Technol. 27, 79–86. doi:10.1016/S0925-5214(02)00186-2

Verboven, P., Flick, D., Nicolaï, B.M., Alvarez, G., 2006. Modelling transport phenomena in refrigerated food bulks, packages and stacks: basics and advances. Int. J. Refrig. 29, 985–997. doi:10.1016/j.ijrefrig.2005.12.010

Wolfe, G.C., Black, J.L., Jordan, R.A. 1993. **The dynamic control of storage atmospheres** CA '93. Proc. 6thIntl. Controlled Atmosphere Research Conference, Cornell Univ., Ithaca, NY, USA Northeast Reg. Agric. Eng. Service, Ithaca, NY, USA (1993), pp. 323-331

Wollin, A.S., Little, C.R. , Packer., J.S. 1985. **Dynamic control of storage atmospheres** S. Blankenship (Ed.), Controlled atmospheres for storage and transport of perishable agricultural commodities. Proc. 4th Natl. Controlled Atmosphere Research Conference, Raleigh, North Carolina Hort. Rept. No. 126. Dept. Hort. Sci., North Carolina State Univ., Raleigh, NY, USA (1985), pp. 308-315

Wright, H., DeLong, J., Harrison, P. a., Gunawardena, A.H.L. a. N., Prange, R., 2010. The effect of temperature and other factors on chlorophyll a fluorescence and the lower O_2 limit in apples (*Malus x domestica* Borkh.). Postharvest Biol. Technol. 55, 21–28. doi:10.1016/j.postharvbio.2009.07.011

Yearsley, C.W., Banks, N.H., Ganesh, S., Cleland, D.J., 1996. Determination of lower O_2 limits for apple fruit. Postharvest Biol. Technol. 8, 95–109. doi:10.1016/0925-5214(96)00064-6

Supplementary material S1: Model simplification using equilibrium assumption

The rates of change of O_2 and CO_2 gas in the intercellular pores compartment are given by:

$$\begin{cases} \varepsilon V_f \dfrac{dc_{\mathrm{O}_2,g}}{dt} = -h_{\mathrm{O}_2,s} A_s \left(c_{\mathrm{O}_2,g} - c_{\mathrm{O}_2,a} \right) - h_{\mathrm{O}_2,cell} A_{cortex} V_f \left(c_{\mathrm{O}_2,g} RTH_{\mathrm{O}_2} - c_{\mathrm{O}_2,cell} \right) \\ \varepsilon V_f \dfrac{dc_{\mathrm{CO}_2,g}}{dt} = -h_{\mathrm{CO}_2,s} A_s \left(c_{\mathrm{CO}_2,g} - c_{\mathrm{CO}_2,a} \right) - h_{\mathrm{CO}_2,cell} A_{cortex} V_f \left(c_{\mathrm{CO}_2,g} RTH_{\mathrm{CO}_2} - c_{\mathrm{CO}_2,cell} \right) \end{cases} \quad \text{(S1)}$$

while the rates of change of concentrations of O_2 and CO_2 in the cells compartment is given by:

$$\begin{cases} (1-\varepsilon) V_f \dfrac{dc_{\mathrm{O}_2,cell}}{dt} = h_{\mathrm{O}_2,cell} A_{cortex} V_f \left(c_{\mathrm{O}_2,g} RTH_{\mathrm{O}_2} - c_{\mathrm{O}_2,cell} \right) + r_{\mathrm{O}_2} (1-\varepsilon) V_f \\ (1-\varepsilon) V_f \dfrac{dc_{\mathrm{CO}_2,c}}{dt} = h_{\mathrm{CO}_2,cell} A_{cortex} V_f \left(c_{\mathrm{CO}_2,g} RTH_{\mathrm{CO}_2} - c_{\mathrm{CO}_2,cell} \right) + r_{\mathrm{CO}_2} (1-\varepsilon) V_f + S_{\mathrm{CO}_2} (1-\varepsilon) V_f \end{cases} \quad \text{(S2)}$$

Rewriting the equations of the cells compartment (S2) to explicitate the transfer term between pore and cell compartments results in:

$$\begin{cases} h_{\mathrm{O}_2,cell} A_{cortex} V_f \left(c_{\mathrm{O}_2,g} RTH_{\mathrm{O}_2} - c_{\mathrm{O}_2,cell} \right) = (1-\varepsilon) V_f \dfrac{dc_{\mathrm{O}_2,cell}}{dt} - r_{\mathrm{O}_2} (1-\varepsilon) V_f \\ h_{\mathrm{CO}_2,cell} A_{cortex} V_f \left(c_{\mathrm{CO}_2,g} RTH_{\mathrm{CO}_2} - c_{\mathrm{CO}_2,cell} \right) = (1-\varepsilon) V_f \dfrac{dc_{\mathrm{CO}_2,cell}}{dt} - r_{\mathrm{CO}_2} (1-\varepsilon) V_f - S_{\mathrm{CO}_2} (1-\varepsilon) V_f \end{cases} \quad \text{(S3)}$$

Substitution of the transfer terms (S3) in the equations for the pores compartment (S1) and assuming equilibrium between the gas concentrations in the pore and cell compartments ($\dfrac{dc_{i,cell}}{dt} = \dfrac{dc_{i,g}}{dt} RTH$) results in:

$$\begin{cases} \varepsilon V_f \dfrac{\partial c_{\mathrm{O_2},g}}{\partial t} = -h_{\mathrm{O_2},s} A_{\mathrm{s}} \left(c_{\mathrm{O_2},g} - c_{\mathrm{O_2},a} \right) - \left(1-\varepsilon\right) V_f \dfrac{dc_{\mathrm{O_2},g}}{dt} RTH_{\mathrm{O_2}} + r_{\mathrm{O_2}} \left(1-\varepsilon\right) V_f \\ \varepsilon V_f \dfrac{\partial c_{\mathrm{CO_2},g}}{\partial t} = -h_{\mathrm{CO_2},s} A_{\mathrm{s}} \left(c_{\mathrm{CO_2},g} - c_{\mathrm{CO_2},a} \right) - \left(1-\varepsilon\right) V_f \dfrac{dc_{\mathrm{CO_2},g}}{dt} RTH_{\mathrm{CO_2}} + r_{\mathrm{CO_2}} \left(1-\varepsilon\right) V_f + S_{\mathrm{CO_2}} \left(1-\varepsilon\right) V_f \end{cases} \quad \text{(S4)}$$

Finally rearranging delivers:

$$\begin{cases} \left(\varepsilon + RTH_{\mathrm{O_2}} \left(1-\varepsilon\right) \right) V_f \dfrac{dc_{\mathrm{O_2},g}}{dt} = -h_{\mathrm{O_2},s} A_{\mathrm{s}} \left(c_{\mathrm{O_2},g} - c_{\mathrm{O_2},a} \right) + r_{\mathrm{O_2}} \left(1-\varepsilon\right) V_f \\ \left(\varepsilon + RTH_{\mathrm{CO_2}} \left(1-\varepsilon\right) \right) V_f \dfrac{dc_{\mathrm{CO_2},g}}{dt} = -h_{\mathrm{CO_2},s} A_{\mathrm{s}} \left(c_{\mathrm{CO_2},g} - c_{\mathrm{CO_2},a} \right) + r_{\mathrm{CO_2}} \left(1-\varepsilon\right) V_f + S_{\mathrm{CO_2}} \left(1-\varepsilon\right) V_f \end{cases} \quad \text{(S5)}$$